The Sea-Breeze Front Analytical Model

YIZHAK FELIKS

Israel Institute for Biological Research, Department of Mathematics, Ness-Ziona, Israel

(Manuscript received 2 February 1987, in final form 12 October 1987)

ABSTRACT

Analytical solutions to the nonlinear equations of motion are used to describe the sea breeze front.

It is found that the front can develop when the atmosphere stratification in the heated layer is neutral or unstable. The temperature drop due to front passage is proportional to the square of the difference between the front speed and the synoptic wind. This square of the difference, on the other hand, is proportional to $[2\theta(\bar{s})/\theta_m]ga$ where $\theta(\bar{s})$ is the mean potential temperature drop across the front and a is the front radius. Fronts which have the same speed of propagation and size, have a larger temperature drop when the synoptic wind blows in the opposite direction to the direction of propagation.

Onshore winds associated with strong convergence are obtained in the lower part of the front, while the return current associated with strong divergence is observed in the upper part. The vertical velocity reaches values of some meters per second in the front region.

The front propagation is studied in terms of the vorticity equation. The buoyancy term always tends to propagate the front inland. The nonlinear advective term in most of the cases tends to slow this propagation. In some of the cases when buoyancy is very low the advective term tends to propagate the front inland.

1. Introduction

The sea breeze has been extensively studied by observations and dynamic models (Atkinson, 1981).

A most significant feature is the sea breeze front. It is usually defined by an abrupt change in wind intensity, manifested in a horizontal convergence of the air flow. This convergence causes the ascent of air over the front, while air descends on the seaward side of the front. There is a marked slope (seaward) of the isothermal surfaces.

The front has a rather limited lateral extent. Wallington (1960), according to an observation made in the south of England, describes it as a narrow zone of 100–200 m, which has an uplift of about 2–9 m s^{-1}. A most detailed description of the front is given by Simpson et al. (1977). A rather complex structure emerges in which the fronts, having raised heads (about 600 m high) are twice the depth of the following flow. The fronts have a speed of 2–8 m s^{-1}. Physick (1976) concludes that the front at night moved faster than during the day. The speed of the fronts has a large variability.

A few observations have been made about the relationship between the sea breeze and the vertical stability. Wexler (1948), Pearce (1968), Johnson and O'Brien (1973) and Brittain (1978) claim that in a stable atmosphere the upper stable layers act as a strong damping mechanism on the vertical circulation of the sea breeze. A less stable or unstable atmosphere encourages an extension of the circulation both horizontally, and vertically, as well as an increase in intensity (Atkinson, 1981).

In nonlinear numerical models of the sea breeze circulation, weak fronts develop. These fronts, identified by horizontal convergence, are associated with a maximum of uplift motions. Neumann and Mahrer (1974) observed a warm dome over the front region, while the cool air from the sea was observed behind the front. A similar warm dome was also observed in the numerical simulations of the breeze by Estoque (1962). The speed of the front was 2.2 m s^{-1}. Pearson (1973) studied the properties of the breeze front by a simple numerical model. He found that the speed of the front was constant after the heat flux ceased. It was independent of the initial potential temperature profile, the vertical distribution of heat and the manner in which a final potential temperature profile was obtained.

In all of the numerical models the vertical velocities are smaller by an order of magnitude and the front spreads over an area which is larger by an order of magnitude in comparison to the observations. This is probably due to a horizontal grid spacing of, 1–5 km, which is too large to specify the sea breeze front in more detail. Because the numerical models describe one or a few simulations of the sea breeze it is not clear what the environmental parameters are and how they influence the front intensity, speed of propagation, and horizontal and vertical extent.

Corresponding author address: Dr. Yizhak Feliks, Institute for Biological Research, P.O. Box 19, 70450 Ness-Ziona, ISRAEL.

It has been found that the following analytical solution to the nonlinear, nonhydrostatic equations of motion serves to describe the sea breeze front. This solution enables us to study in detail the parameters which influence the sea breeze front and the causes of its propagation inland.

2. Formulation of the problem

The sea breeze and its front are limited to the lower atmosphere. Hence its height is much smaller than the height scale of the atmosphere. This allows us to use the Boussinesq incompressible approximation of the equations of motions.

$$\frac{\partial u}{\partial t} + u\frac{\partial u}{\partial x} + w\frac{\partial u}{\partial z} = -\frac{1}{\rho_m}\frac{\partial P}{\partial x} \tag{2.1}$$

$$\frac{\partial w}{\partial t} + u\frac{\partial w}{\partial x} + w\frac{\partial w}{\partial z} = -\frac{1}{\rho_m}\frac{\partial P}{\partial z} - \frac{\rho g}{\rho_m} \tag{2.2}$$

$$\frac{\partial u}{\partial x} + \frac{\partial w}{\partial z} = 0. \tag{2.3}$$

Here $u = u' + U$, U is the large scale wind, u' and w are the perturbation velocity components, ρ_m is a mean reference density, P and ρ are the perturbation pressure and density. For purposes of simplicity the Coriolis force and viscosity effects are omitted. Pearson (1973) shows that the speed of the front was slightly influenced by viscosity and was independent of the Coriolis parameter until half-pendulum day.

The thermodynamic equation is

$$\frac{\partial \sigma}{\partial t} + u\frac{\partial \sigma}{\partial x} + w\frac{\partial \sigma}{\partial z} = 0$$

$$\sigma = \sigma' + N^2 z. \tag{2.4}$$

Here

$$N^2 = \frac{g}{\rho_m}\frac{\partial \bar{\theta}}{\partial z}$$

is the Brunt–Väisälä frequency, $\bar{\theta}$ is the reference potential temperature and

$$\sigma = \frac{-\rho g}{\rho_m} = \frac{g\theta}{\theta_m} \tag{2.5}$$

is the buoyancy force; θ is the perturbation potential temperature from its value at the lower boundary.

Pearson (1973) shows that the final front structure and its speed are independent of the time history of the temperature profile; only the final temperature profile is important. In our case we are dealing with the final front.

As the fluid is incompressible a streamfunction will be introduced, where

$$u = -\frac{\partial \Psi}{\partial z}, \quad w = \frac{\partial \Psi}{\partial x}. \tag{2.6}$$

Cross-differentiation of (2.1) and (2.2) will eliminate the pressure leading to the vorticity equation

$$\frac{\partial \zeta}{\partial t} + u\frac{\partial \zeta}{\partial x} + w\frac{\partial \zeta}{\partial z} = \frac{\partial \sigma}{\partial x} \tag{2.7}$$

$$\zeta = \frac{\partial w}{\partial x} - \frac{\partial u}{\partial z} = \nabla^2 \Psi. \tag{2.8}$$

To analytically solve the above nonlinear equations we assume that the speed of the front is constant and that the front maintains its structure.

The transformation of the x-coordinate to the $s = x - ct$ coordinate, where c is the front speed, enables us to eliminate the time derivative from equations (2.4) and (2.7), i.e.

$$J(\Psi + cz, \zeta) - \frac{\partial \sigma}{\partial s} = 0 \tag{2.9}$$

$$J(\Psi + cz, \sigma) = 0 \tag{2.10}$$

where J is the Jacobian operator

$$J(f, g) = \frac{\partial f}{\partial s}\frac{\partial g}{\partial z} - \frac{\partial f}{\partial z}\frac{\partial g}{\partial s}.$$

In Fig. 1, a diagram of the frontal region in the moving coordinates is shown.

We look for a solution to (2.9) and (2.10) in the region $z < b$, $s > 0$. This solution has to fulfill the following boundary conditions: 1) $w = 0$ on $z = 0$, and 2) in the horizontal velocity, u, a free-slip condition is

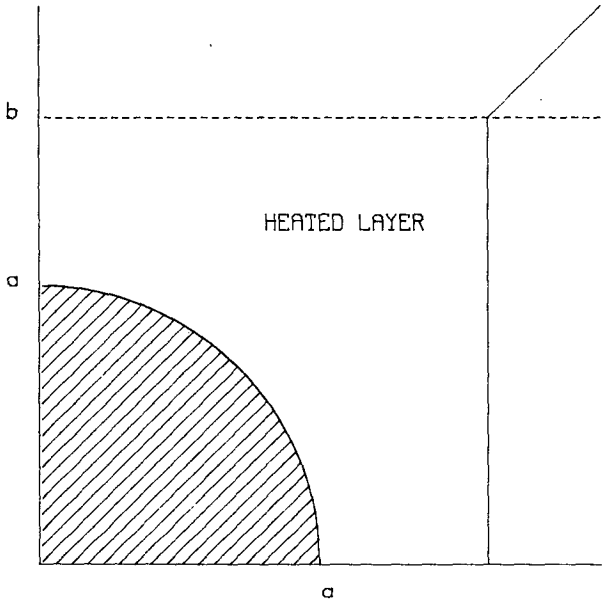

FIG. 1. Diagram of the frontal region in the moving coordinates (s, z). b is the height of the heated layer. The shaded quarter of circle on the left side represents the frontal area whose radius is a. The final potential temperature profile is shown on the right side.

assumed. The front is local; i.e., $x \to \infty$: $u = U$, $w = 0$, $\Psi = -Uz$

$$\left.\begin{aligned} \frac{\partial \sigma}{\partial z} &= N_b^2, \quad z < b \\ \frac{\partial \sigma}{\partial z} &= N^2, \quad z > b \end{aligned}\right\} \tag{2.11}$$

where N_b is the Brunt–Väisälä frequency in the heated layer whose depth is b.

On the front boundary $r = a$ (Fig. 1), $\Psi + cz = 0$. Since particles move on lines of constant $\Psi + cz$, when viewed in the reference frame (s, z), this definition implies that the front carries particles with it as it propagates. This also indicates that there is no mass-flux through the front boundary. On this boundary Ψ, w, u and σ are continuous.

Because the Jacobian in (2.10) vanishes, there is an arbitrary functional dependence between $\Psi + cz$ and σ. Assume this function is piecewise-linear, i.e.

$$\left.\begin{aligned} \sigma &= \gamma_I(\Psi + cz), \quad r < a \\ \sigma &= \gamma_E(\Psi + cz), \quad r > a \end{aligned}\right\}. \tag{2.12}$$

In (2.12) the transition from one portion of the broken line to another is accomplished as a function of the distance r from the coordinate origin, rather than the value of the argument $\Psi + cz$. Thus a has to be chosen in the following manner:

$$\left.\begin{aligned} \Psi + cz &< 0, \quad r < a \\ \Psi + cz &> 0, \quad r > a \end{aligned}\right\}. \tag{2.13}$$

This condition also assures continuity of the buoyancy, σ, as we move from one portion of the broken line to another. The other choice $\Psi + cz > 0$, when $r < a$, leads to very small horizontal winds in the front since $u = -\partial\Psi/\partial z < c$. We note that the shape of the front as given by the curve $\Psi + cz = 0$ is an assumption of the theory.

Substituting (2.11) into (2.12) we get

$$\sigma \underset{x \to \infty}{\to} \gamma_E(c - U)z = N_b^2 z. \tag{2.14}$$

Assuming $c - U < 0$, from (2.14) we find that σ and γ_E has an opposite sign, while from (2.12) and (2.13) they have the same sign. So only the case

$$c - U > 0 \tag{2.15}$$

is possible; i.e., the speed of the front is larger than the speed of the synoptic wind U.

When substituting (2.12) into (2.9) we get

$$\begin{aligned} J(\Psi + cz, \zeta - \gamma_I z) &= 0, \quad r < a \\ J(\Psi + cz, \zeta - \gamma_E z) &= 0, \quad r > a. \end{aligned} \tag{2.16}$$

Since the Jacobian in (2.16) vanishes there is arbitrary functional dependence between $\Psi + cz$ and

$$\begin{aligned} &\zeta - \gamma_I z, \quad r < a \\ &\zeta - \gamma_E z, \quad r > a \end{aligned}$$

assuming this function is piecewise-linear, i.e.

$$\begin{aligned} \nabla^2\Psi - \gamma_I z &= -k^2(\Psi + cz), \quad r < a \\ \nabla^2\Psi - \gamma_E z &= p^2(\Psi + cz), \quad r > a \end{aligned} \tag{2.17}$$

or

$$\begin{aligned} \nabla^2\Psi + k^2\Psi &= (\gamma_I - k^2 c)z, \quad r < a \\ \nabla^2\Psi - p^2\Psi &= (\gamma_E + p^2 c)z, \quad r > a. \end{aligned} \tag{2.18}$$

To solve (2.18), we transfer to polar coordinates $s = r\cos\alpha$, $z = r\sin\alpha$. The equation (2.18) in the new coordinate system has the form:

$$\left.\begin{aligned} &\frac{1}{r}\frac{\partial}{\partial r}\left(r\frac{\partial \Psi}{\partial r}\right) + \frac{1}{r^2}\frac{\partial^2 \Psi}{\partial \alpha^2} + k^2\Psi \\ &\qquad = (\gamma_I - k^2 c)r\sin\alpha, \quad r < a \\ &\frac{1}{r}\frac{\partial}{\partial r}\left(\frac{\partial \Psi}{\partial r}\right) + \frac{1}{r^2}\frac{\partial^2 \Psi}{\partial \alpha^2} - p^2\Psi \\ &\qquad = (\gamma_E + p^2 c)r\sin\alpha, \quad r > a \end{aligned}\right\}. \tag{2.19}$$

First we deal in the region $r > a$. A particular solution of (2.19) is

$$\Psi_{NH} = \frac{\gamma_E + p^2 c}{p^2} r\sin\alpha.$$

The solution of the homogeneous equation is obtained by the separation of variables:

$$\left.\begin{aligned} \Psi_H &= f(r)h(\alpha) \\ \frac{r}{f}\frac{\partial}{\partial r}\left(r\frac{\partial f}{\partial r}\right) - r^2p^2 &= 1 = -\frac{1}{h}\frac{\partial^2 h}{\partial \alpha^2} \end{aligned}\right\}; \tag{2.20}$$

thus $h(\alpha) = \sin\alpha$, $f(r) = BK_1(rp)$, $\Psi_H = BK_1(rp)\sin\alpha$, where K_1 is the modified Bessel function of the first order and second kind. Here K_1 is the appropriate solution, since it decays rapidly away from the front. The solution to (2.19) is

$$\Psi = \left(BK_1(rp) - \frac{\gamma_E + p^2 c}{p^2} r\right)\sin\alpha. \tag{2.21}$$

Utilizing the boundary condition (2.11) for $x \to \infty$ we obtain

$$\frac{\gamma_E + p^2 c}{p^2} = U \tag{2.22}$$

$$\frac{\gamma_E}{p^2} = U - c. \tag{2.23}$$

Using (2.15) we get $\gamma_E < 0$. From (2.12) and (2.13) we get

$$\sigma \leqslant 0, \quad r > a \tag{2.24}$$

and far inland according to (2.14)

$$\gamma_E(c - U) = N_b^2 \leqslant 0. \tag{2.25}$$

The last result can be interpreted as follows: A local front can be obtained when the atmosphere stability in the heated layer ($z < b$) is unstable or neutral. In the sea breeze case we will deal in atmosphere whose stability is almost neutral, i.e., $\gamma_E \sim 0$. Notice that in observations significant breezes were observed when the atmosphere stratification was neutral or even unstable. For reference, see the Introduction.

Utilizing the boundary condition on $r = a$

$$\Psi + cz = \Psi + ac \sin\alpha = 0,$$

we obtain

$$B = \frac{\gamma_E}{p^2} \frac{a}{K_1(pa)} \tag{2.26}$$

$$\Psi = (U - c)a\left[\frac{K_1(pr)}{K_1(pa)} - \frac{r}{a}\right] \sin\alpha - cr \sin\alpha. \tag{2.27}$$

In the region $r < a$, particular solution of (2.19) is

$$\Psi_{NH} = \frac{\gamma_I - ck^2}{k^2} r \sin\alpha.$$

The solution to the homogeneous equation is obtained by separating variables in a similar way to (2.19) where $r > a$. Thus, we obtain $\Psi_H = AJ_1(kr) \sin\alpha$, where J_1 is a Bessel function of the first order and kind. The solution to (2.19) is

$$\Psi = \left(AJ_1(kr) + \frac{\gamma_I - ck^2}{k^2} r\right) \sin\alpha. \tag{2.28}$$

Utilizing the boundary condition on $r = a$

$$\Psi = cz = \Psi + ac \sin\alpha = 0,$$

we obtain

$$A = -\frac{\gamma_I}{k^2} \frac{a}{J_1(ka)} \tag{2.29}$$

$$\Psi = \frac{\gamma_I a}{k^2}\left[-\frac{J_1(kr)}{J_1(ka)} + \frac{r}{a}\right] \sin\alpha - cr \sin\alpha. \tag{2.30}$$

On $r = a$ it is clear that Ψ is continuous. We require the same for u and w and thus $\partial\Psi/\partial r$ has to be continuous after some mathematical manipulation. Using the identities, $K_1'(y) = K_1(y)/y - K_2(y)$, $J_1'(y) = J_1(y)/y - J_2(y)$ we obtain the following relationship

$$\frac{\gamma_I}{c - U} \frac{a}{k} \frac{J_2(ka)}{J_1(ka)} = pa \frac{K_2(pa)}{K_1(pa)}. \tag{2.31}$$

Since we are modeling a neutral atmosphere i.e., $\gamma_E \sim 0$, (2.23) can be fulfilled only if $p \sim 0$ also. In this case the right-hand side of (2.31) can be replaced by the

$$\lim_{pa \to 0} pa \frac{K_2(pa)}{K_1(pa)} \tag{2.32}$$

as $pa \to 0$ the following approximation takes place [Abramowitz and Stegun (1970), p. 375]

$$K_n(pa) \sim \frac{1}{2} \Gamma(n)\left(\frac{pa}{2}\right)^{-n}, \quad n = 1, 2 \tag{2.33}$$

where Γ is a gamma function, so

$$\lim_{pa \to 0} pa \frac{K_2(pa)}{K_1(pa)} = 2 \frac{\Gamma(2)}{\Gamma(1)} = 2. \tag{2.34}$$

Substituting (2.34) into (2.31), we obtain

$$\gamma_I = \frac{2k}{a} \frac{J_1(ka)}{J_2(ka)} (c - U). \tag{2.35}$$

Because the air behind the front is cooler than the air ahead of the front, σ in $r < a$ is lower (more negative) than σ in $r > a$. Thus we conclude from (2.12) and (2.13) that $\gamma_I > 0$, and consequently we can further conclude from (2.35) that

$$J_1(ka) \geq 0, \quad 0 \leq ka \leq 3.83171. \tag{2.36}$$

It is important to note that (2.36) is the only range of ka which is possible; for other ranges of ka where: $J_1(ka)/J_2(ka) \geq 0$, $\Psi + cz$ change its sign in $0 < ra < ka$ in contradiction to (2.13).

3. Potential temperature in the front

As we have shown above in the region where $r > a$, the vertical stratification is almost neutral, i.e., $\sigma \sim 0$.

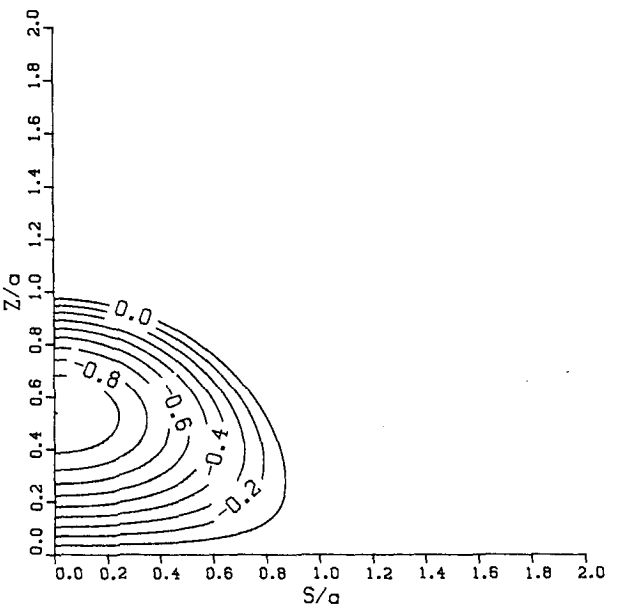

FIG. 2. Isolines of the functional structure of: the buoyancy and the potential temperature normalized by its maximum, as a function of nondimensional moving coordinates s/a, z/a.

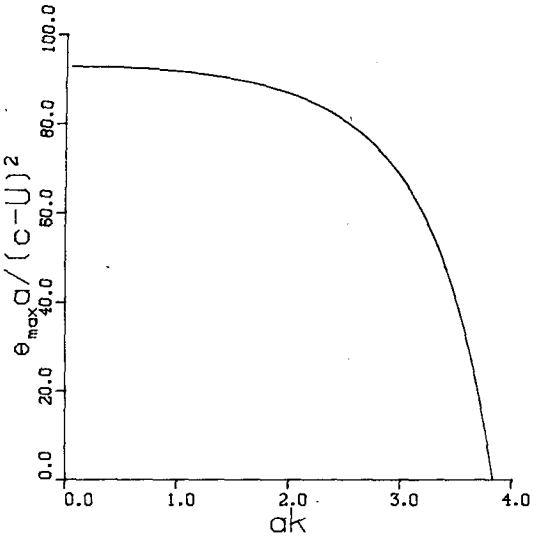

FIG. 3. The maximum potential temperature drop due to passage of the front normalized by $(c - U)^2/a$ as a function of ka.

In the region $r < a$ using (2.12) and (2.30) we get

$$\sigma = \frac{\gamma_1^2 a}{k^2}\left[\left(-\frac{J_1(kr)}{J_1(ka)} + \frac{r}{a}\right)\sin\alpha\right] \tag{3.1}$$

substituting (2.5) and (2.35) into (3.1) we get

$$\theta = \frac{(c-U)^2}{a}\frac{4\theta m}{g}\left(\frac{J_1(ka)}{J_2(ka)}\right)^2\left[\left(-\frac{J_1(kr)}{J_1(ka)} + \frac{r}{a}\right)\sin\alpha\right]. \tag{3.2}$$

The expression in the square brackets in (3.1) and (3.2) is nondimensional and describes the structure of the buoyancy and potential temperature at the front. In Fig. 2, this function, normalized by its maximum, is shown in the nondimensional coordinates s/a, z/a for $ka = 2.6$, note that this figure shows the potential temperature also for $r > a$, since both σ and $\theta \approx 0$ for $r > a$. We note that the feature of this function is similar to the range of ka given in (2.36). The differences are less than 10%. The structure function of the potential temperature, as shown in Fig. 2, resembles the structure observed by Simpson et al. (1977) where $a = 800$ m. The largest gradient in the potential temperature is observed at a height of 400 m, this gradient is significantly larger than near the ground. This feature is also obtained in our model. However, the gradient in the first tens of meters, adjacent to the ground, is smaller than in observations; this is due to lack of friction in our model.

The maximum of θ, θ_{max}, is determined by the maximum of the structure function times the amplitude of it [the term outside the square brackets in (3.2)]. In Fig. 3, $\theta_{max}a/(c - U)^2$ is shown as a function of ka. To determine the value of ka, one has to know the maximum fall in temperature due to passage of the front, the radius of the front, its speed of propagation and the speed of the synoptic wind.

Temperature drop due to passage of the front, is proportional to $(c - U)^2$ when ka remains constant. So fronts with the same speed of propagation and the same radius have a larger temperature drop when the synoptic wind is weak or blows in the opposite direction to front propagation (offshore). Atkinson (1981), in observations noticed similar results. Some values of θ_{max}, a, c, U and ka are given in Table 1, as obtained from our model. These values are similar to observations.

The integral of (3.2) over the front area is

$$\iint \theta dA = \frac{(c-U)^2}{a}\frac{4\theta_m}{g}\left(\frac{J_1(ka)}{J_2(ka)}\right)^2 \times \int_0^{\pi/2}\int_0^a \left(\frac{-rJ_1(kr)}{J_1(ka)} + \frac{r^2}{a}\right)\sin\alpha dr d\alpha. \tag{3.3}$$

Using the identity $yJ_1(y) = -yJ_0'(y)$ and integrating by parts we get:

$$(c-U)^2 = \iint \theta dA \frac{4g}{a\theta_m}\frac{2}{\pi}\Big/\left(\frac{J_1(ka)}{J_2(ka)}\right)^2 \times \left[\frac{1}{ka}\left(H_0(ka) - \frac{J_0(ka)}{J_1(ka)}H_1(ka)\right) - \frac{1}{3}\right] \tag{3.4}$$

where H_0, H_1 are Struve functions.

From the mean value theorem for definite integrals, we have:

TABLE 1.

a (m)	U (m s^{-1})	c (m s^{-1})	θ_{max} (°C)	ka	u_{max} (m s^{-1})	u_{min} (m s^{-1})	w_{max} (m s^{-1})	$k^2c - \gamma_1$ (m^{-1} s^{-1})	γ_1 (m^{-1} s^{-1})
700	−3	2	3.2	1	8	−7	5	$-1.51 \cdot 10^{-4}$	$1.55 \cdot 10^{-4}$
700	2	4	0.5	1	4.8	−1.6	2	$-5.38 \cdot 10^{-5}$	$6.20 \cdot 10^{-5}$
700	−3	2	2.7	2.6	8	−7	5	$-7.24 \cdot 10^{-5}$	$1.00 \cdot 10^{-4}$

u_{max}: maximum speed of u.
u_{min}: minimum speed of u.
w_{max}: maximum speed of w.

$$\iint \theta dA = \theta(\bar{s}) \frac{\pi a^2}{4},$$

$\bar{s}$ is a point in the front and:

$$(c - U)^2 = \frac{2\theta(\bar{s})}{\theta_m} ga \Big/ \left(\frac{J_1(ka)}{J_2(ka)}\right)^2 \times \left[\frac{1}{ka}\left(H_0(ka) - \frac{J_0(ka)}{J_1(ka)} H_1(ka)\right) - \frac{1}{3}\right] \quad (3.5)$$

i.e., the square of the speed of the front relative to the synoptic wind is proportional to the mean drop of θ over the front area $[\theta(\bar{s})]$ times the front height. This result, within constant factors, is the same as the known results on density currents (Benjamin, 1968). So fronts with lower temperature drop can propagate faster if their radius is sufficiently large.

4. The winds in the front

An analytical expression of the horizontal and vertical velocities can be obtained from (2.6),

$$\left.\begin{aligned} u - c &= -\frac{\partial \Psi}{\partial z} - c = -\left(\frac{\partial \Psi}{\partial r}\frac{\partial r}{\partial z} + \frac{\partial \Psi}{\partial a}\frac{\partial \alpha}{\partial z}\right) - c \\ w &= \frac{\partial \Psi}{\partial s} = \frac{\partial \Psi}{\partial r}\frac{\partial r}{\partial s} + \frac{\partial \Psi}{\partial \alpha}\frac{\partial \alpha}{\partial s} \end{aligned}\right\}, \quad (4.1)$$

(2.25), (2.28) and the trigonometric identity $(\arctan y)' = 1/(1 + y^2)$. After some mathematical manipulation we have

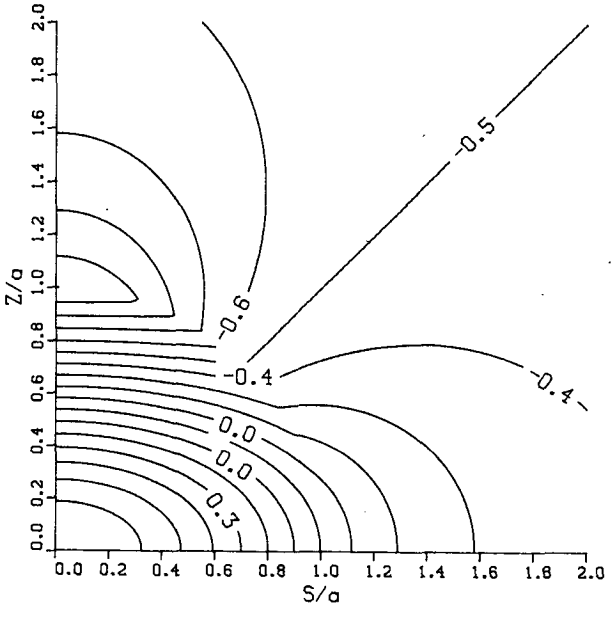

FIG. 4. Isolines of the structure function of the horizontal velocity relative to the front speed normalized by its maximum as a function of the nondimensional moving coordinates s/a, z/a.

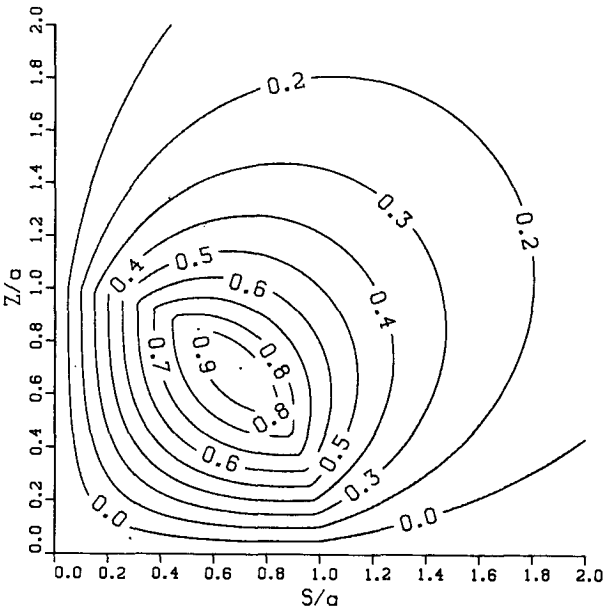

FIG. 5. Isoline of the vertical velocity normalized by its maximum as a function of the nondimensional moving coordinates s/a, z/a.

for $r < a$:

$$u - c = (c - U) \times \left[\frac{J_1(kr)}{kr} - J_2(kr)\sin^2\alpha - \frac{J_1(ka)}{ka}\frac{2}{J_2(ka)}\right] \quad (4.2)$$

$$w = (c - U)\left[2\frac{J_2(kr)}{J_2(ka)}\sin\alpha\cos\alpha\right] \quad (4.3)$$

for $r > a$:

$$u - c = (c - U)\left[\frac{a}{r}\frac{K_1(pr)}{K_1(pa)} - \frac{paK_2(pr)}{K_1(pa)}\sin^2\alpha - 1\right] \quad (4.4)$$

$$w = (c - U)\left[pa\frac{K_2(pr)}{K_1(pa)}\sin\alpha\cos\alpha\right]. \quad (4.5)$$

The expression in square brackets in (4.2)–(4.5) is nondimensional and describes the structure of the horizontal and vertical velocities at the front. In Figs. 4 and 5 the structure functions are shown for $u - c$, and w, in the nondimensional coordinates s/a, z/a, for $ka = 2.6$, $pa = 10^{-3}$. The feature of this function is similar to other values of ka in the range given in (2.36).

In the horizontal velocity, u, (Fig. 4) an abrupt change in wind intensity is evident. The largest velocities can be observed near the ground behind the strong convergence zone. The return current is observed at altitudes above the vortex center ($z/a > 0.5$, this height also depends on the value of c), and causes a divergence zone. This zone is located above the lower convergence zone. Some values of the maximum and minimum of

the horizontal wind speed in the front are given in Table 1.

In the vertical velocity (Fig. 5) upward motions are observed over the front. The height at which the maximum is found is the boundary between the convergence and divergence zone observed in the horizontal velocity. Some values of the maximum speed of the vertical velocity are given in Table 1. The horizontal and vertical winds predicted by the model are similar to observations documented by Atkinson (1981), except in the first tens of meters adjacent to the ground. This is due to the lack of friction and the free-slip condition assumed in the lower boundary.

The sharp change in $u - c$ and w observed in Figs. 4 and 5 at $r = a$, is a result of discontinuity in the vorticity at this boundary.

5. The causes of front propagation

The causes of front propagation are studied in terms of the vorticity equation. An analytical expression of the vorticity in the front can be obtained from (2.17)

1) $r < a$:

$$\zeta = \nabla^2\Psi = k^2\Psi + (\gamma_I - k^2c)z. \tag{5.1}$$

Substituting Ψ from (2.28) into (5.1) we get

$$\zeta = \left[\frac{J_1(kr)}{J_2(ka)}\, 2ka \sin\alpha\right]\frac{c - U}{a} \tag{5.2}$$

2) for $r > a$:

$$\zeta = \nabla^2\Psi = p^2\Psi + (\gamma_E + p^2c)z. \tag{5.3}$$

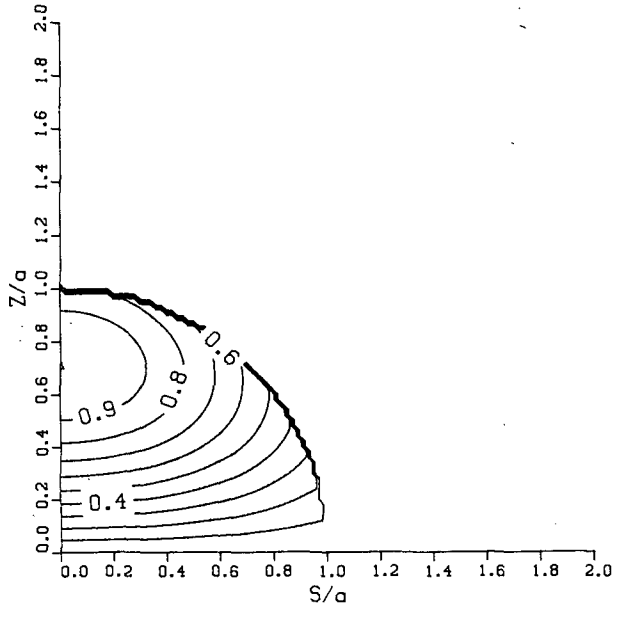

FIG. 6. As in Fig. 5 but for the vorticity.

Substituting Ψ from (2.27) into (5.3) we get

$$\zeta = \frac{\gamma_E}{p}\, pa\, \frac{K_1(pr)}{K_1(pa)} \sin\alpha. \tag{5.4}$$

The vorticity in the region $r > a$ is very small since γ_E/p is very small. In the region $r < a$ the vorticity has a positive sign and its maximum is obtained at $\alpha = \pi/2$. The structure function of the vorticity is given by the expression in the square brackets in (5.2). In Fig. (6), this structure function normalized by its maximum, is shown for $ka = 2.6$. This feature is similar for the range of ka given in (2.36).

Examination of the vorticity equation (2.7) shows that two terms cause changes in the vorticity, the nonlinear advective term $-J(\Psi, \zeta)$ and the horizontal gradient of the buoyancy (or potential temperature) $\partial\sigma/\partial x$. A positive horizontal gradient of the buoyancy tends to increase the vorticity and a negative one to decrease the vorticity. Across the front, $\partial\sigma/\partial x > 0$, and this term tends to propagate the front inland.

The analytical expressions for the two tendency terms are

$$-J(\Psi, \zeta) = -J[\Psi, -k^2\Psi + (\gamma_I - k^2c)z]$$

$$= \frac{\partial\Psi}{\partial x}(k^2c - \gamma_I) = w(k^2c - \gamma_I) \tag{5.5}$$

$$\frac{\partial\sigma}{\partial x} = \frac{\partial}{\partial x}[\gamma_I(\Psi + cz)] = \frac{\partial\Psi}{\partial x}\gamma_I = w\gamma_I. \tag{5.6}$$

The sum of the two terms gives

$$\frac{\partial\zeta}{\partial t} = wk^2c. \tag{5.7}$$

Since w is positive everywhere, the right-hand side of (5.7) is positive and causes the eastward propagation of the front.

The contribution of the nonlinear advective term to the vorticity depends on the sign of $k^2c - \gamma_I$. When this sign is negative, the advection term decreases the vorticity and so inhibit the propagation of the front, and vice versa when its sign is positive. To evaluate this coefficient substitute (2.33) instead of γ_I

$$k^2c - \gamma_I = \frac{kc}{a}\left[ka - \frac{J_1(ka)}{J_2(ka)}\, 2\,\frac{c - U}{c}\right]. \tag{5.8}$$

In Fig. 7 the value of the term in the square brackets is given as a function of ka and $(c - U)/c$. Some values of $k^2c - \gamma_I$ and γ_I are given in Table 1. In most of the cases the advection term has a negative sign due to advection of particles with low vorticity into a region of higher vorticity, and so this term slows the inland propagation of the front. When the buoyancy is very low the advection term is positive. This is due to the advection of particles with high vorticity into the region

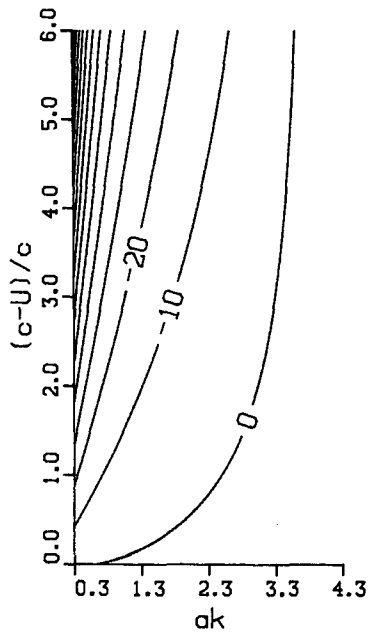

FIG. 7. Isolines of $\{ka - [J_1(ka)/J_2(ka)]2(c - U/c)\}$ i.e., the coefficient of the nonlinear advective term normalized by kc/a [see (5.8)] as a function of $(c - U)/c$ and ka.

of lower vorticity. Thus, the advection tends to propagate the front inland.

6. Summary

An analytical solution to the nonlinear equations of motion serves to describe the sea breeze front. This solution assumes that the front has a constant speed of propagation, and that the front maintains its structure.

The requirement that the front is local leads to the result that the front can develop when the atmosphere has neutral or even unstable stratification. Such stratification was observed in many cases where significant breezes developed. This stratification was caused by diabatic heating of the lower part of the atmosphere over the land. Our model does not intend to predict this process. The model deals in that time interval after the atmosphere has already been heated and consequently the stratification in the heated layer is neutral.

The thermal field in the front can be described by a nondimensional structure function, which is similar to all fronts. The amplitude of this function is proportional to the square of the difference between the front speed and the synoptic wind. Thus sharper fronts are obtained when synoptic wind blows in the opposite direction to that of the front propagation (when the speed and size of the front remain constant). On the other hand the square of the speed of the front relative to the synoptic wind, is proportional to

$$\frac{2\theta(\bar{s})}{\theta_m} ga$$

where $\theta(\bar{s})$ is the mean potential temperature drop across the front area and a is the front radius. This is the same as the known results on density currents. So fronts with smaller temperature drop can propagate faster if their radius is sufficiently large. The temperature drop due to passage of the front as predicted by the model is similar to the temperature drop observed, except for the first tens of meters adjacent to the ground. The reason for these differences is derived from the lack of friction in our model.

The horizontal and vertical velocity in the front, can be described by nondimensional structure functions which are similar to all fronts, while their amplitudes are proportional to the speed of the front relative to the synoptic wind. Onshore winds associated with strong convergence are observed in the lower part of the front, while in the upper part of the front the return current is observed, and it is associated with strong divergence.

An upward motion is observed over the front. The feature of the vertical wind is associated with the convergence and divergence of the horizontal wind. The speed of the horizontal and vertical wind predicted by the model, is similar to the observation, except for the first tens of meters adjacent to ground, where the "slippery" condition in the lower boundary and lack of friction cause those differences.

To match the flow behind the front onto this solution, we assume that the seabreeze has uniform horizontal flow in the vertical axis, i.e., $\partial\sigma/\partial s = 0$ in $s < 0$. In that case we note that the front solution is not consistent with the entirely horizontal flow behind $s < 0$ since the air in the front coming from the left and below $z/a = 0.5$ must acquire its vorticity from buoyancy gradient in $s < 0$. We also note that this solution behind the front is convectively unstable, since the lowest potential temperature is observed at $z/a \sim 0.5$. In a real seabreeze the air behind the front is probably much more statically stable due to $\sigma < 0$ at the surface behind the front. In our model this fact cannot be incorporated due to our lower boundary condition, $\sigma = 0$.

The causes of front propagation are studied in terms of the vorticity equation which has the following two terms: one being the horizontal gradient of buoyancy and the other the nonlinear advection. The buoyancy term always tends to increase the vorticity and so tends to propagate the front inland. While the nonlinear advective term in most of the cases advects particles with low vorticity into a region of higher vorticity it causes a decrease in the vorticity and slows the inland propagation of the front. In some cases when the buoyancy is very low the advection increases the vorticity and tends to propagate the front inland.

Acknowledgments. An anonymous reviewer is thanked for careful reading of this paper and for many constructive criticisms.

REFERENCES

Abramowitz, M. and I. A. Stegun, Eds., 1970: *Handbook of Mathematical Functions.* Natl. Bur. Stand. Amer. Math. Soc. 55, 1046 pp.

Atkinson, B. W., 1981: *Meso-scale Atmospheric Circulations,* London, Academic Press, 495 pp.

Benjamin, B., 1968: Gravity currents and related phenomena. *J. Fluid Mech.,* **31,** 209–248.

Brittain, O. W., 1978: Forecasting sea breezes at Eskmeals. *Meteor. Mag.,* **107,** 88–96.

Estoque, M. A., 1962: The sea-breeze as function of the prevailing situation. *J. Atmos. Sci.,* **19,** 244–250.

Johnson, A. Jr., and J. J. O'Brien, 1973: A study of an Oregon sea breeze event. *J. Appl. Meteor.,* **12,** 1267–1283.

Neumann, J., and Y. Mahrer, 1974: Evolution of a sea breeze front; a numerical study. *Bonn Met. Abhl.,* **17,** 481–492.

Pearce, R. P., 1968: The generation of sea-breezes. *Schweiz. Aero-Rev.,* **43,** 195–200.

Pearson, R. A., 1973: Properties of the sea breeze front as shown by numerical model. *J. Atmos. Sci.,* **30,** 1050–1060.

Physik, W., 1976: A numerical model of the sea-breeze phenomenon over a lake or gulf. *J. Atmos. Sci.,* **33,** 2107–2135.

Simpson, J. E., D. A. Mansfield and J. R. Milford, 1977: Inland penetration of sea-breeze fronts. *Quart. J. Roy. Meteor. Soc.,* **103,** 47–76.

Wallington, C. E., 1959: Structure of sea breeze front as revealed by gliding flights. *Weather,* **14,** 263–269.

Wexler, R., 1946: Theory and observations of land and sea breezes. Bull. Amer. Meteor. Soc., **27,** 272–287.